Biochemistry

 Volume 42, Number 21 June 3, 2003

*Articles*

# Structure, Topology, and Dynamics of Myristoylated Recoverin Bound to Phospholipid Bilayers†

Kathleen G. Valentine,‡ Michael F. Mesleh,§ Stanley J. Opella,§ Mitsuhiko Ikura,|| and James B. Ames*,⊥

*Department of Biochemistry and Biophysics, University of Pennsylvania, Philadelphia, Pennsylvania 19104, Department of Chemistry and Biochemistry, University of California, San Diego, La Jolla, California 92093, Division of Molecular and Structural Biology, Ontario Cancer Institute, and Department of Medical Biophysics, University of Toronto, Toronto, Ontario M5G 2M9, Canada, and Center for Advanced Research in Biotechnology, University of Maryland Biotechnology Institute, Rockville, Maryland 20850*

*Received November 27, 2002; Revised Manuscript Received March 19, 2003*

ABSTRACT: Recoverin, a member of the EF-hand protein superfamily, serves as a calcium sensor in retinal rod cells. A myristoyl group covalently attached to the N-terminus of recoverin facilitates its binding to retinal disk membranes by a mechanism known as the $Ca^{2+}$-myristoyl switch. Samples of $^{15}N$-labeled $Ca^{2+}$-bound myristoylated recoverin bind anisotropically to phospholipid membranes as judged by analysis of $^{15}N$ and $^{31}P$ chemical shifts observed in solid-state NMR spectra. On the basis of a $^{2}H$ NMR order parameter analysis performed on recoverin containing a fully deuterated myristoyl group, the N-terminal myristoyl group appears to be located within the lipid bilayer. Two-dimensional solid-state NMR ($^{1}H-^{15}N$ PISEMA) spectra of uniformly and selectively $^{15}N$-labeled recoverin show that the $Ca^{2+}$-bound protein is positioned on the membrane surface such that its long molecular axis is oriented ~45° with respect to the membrane normal. The N-terminal region of recoverin points toward the membrane surface, with close contacts formed by basic residues K5, K11, K22, K37, R43, and K84. This orientation of the membrane-bound protein allows an exposed hydrophobic crevice, near the membrane surface, to serve as a potential binding site for the target protein, rhodopsin kinase. Close agreement between experimental and calculated solid-state NMR spectra of recoverin suggests that membrane-bound recoverin retains the same overall three-dimensional structure that it has in solution. These results demonstrate that membrane binding by recoverin is achieved primarily by insertion of the myristoyl group inside the bilayer with apparently little rearrangement of the protein structure.

More than 200 membrane-targeting proteins involved in signal transduction processes are cotranslationally modified by the covalent linkage of myristic acid to their N-terminus (*1*, *2*). The observation that viral Src protein is oncogenic only when it is myristoylated first highlighted the biological importance of this modification (*3*). The attached myristoyl group serves as a hydrophobic anchor that reversibly and dynamically recruits proteins to membranes during signaling. Myristoylated recoverin, a 23 kDa $Ca^{2+}$ binding protein and member of the EF-hand superfamily (*4*), serves as a membrane-targeting $Ca^{2+}$ sensor in retinal rod cells, and the myristoyl moiety plays a critical role in regulating the phototransduction cascade in vision (*5*, *6*). Recoverin pro-

† This work was supported by NIH Grant EY12347, the Keck Foundation, and a Beckman Young Investigator Award to J.B.A. It utilized the Resource for Solid-State NMR of Proteins supported by Grant P41 RR09793 from the Biomedical Technology Program Division of Research Resources, National Institutes of Health.

* Corresponding author: e-mail, james@carb.nist.gov; phone, (301) 738-6120; fax, (301) 738-6255.

‡ University of Pennsylvania.

§ University of California, San Diego.

|| Ontario Cancer Institute and University of Toronto.

⊥ University of Maryland Biotechnology Institute.

10.1021/bi0206816 CCC: $25.00 
Published on Web 05/08/2003

longs the lifetime of photoexcited rhodopsin by inhibiting rhodopsin kinase only at high $Ca^{2+}$ levels (*7*, *8*). Hence, recoverin is recruited to membranes to control the desensitization of rhodopsin, and the resulting shortened lifetime of photoexcited rhodopsin at low $Ca^{2+}$ levels may promote visual recovery and contribute to the adaptation to background light.

Three-dimensional structures of myristoylated recoverin in solution have been determined by NMR spectroscopy (*9*, *10*). A striking feature of these structures is that there is a large $Ca^{2+}$-induced conformational change. In the $Ca^{2+}$-free protein, the myristoyl group is sequestered in a deep hydrophobic cavity where it is "clamped" by many aromatic residues, allowing the $Ca^{2+}$-free protein to be cytosolic. The binding of two $Ca^{2+}$ ions by the protein leads to the extrusion of the myristoyl group accompanied by a 45° rotation of the two domains of the protein; this exposes many hydrophobic residues that contact the myristoyl group in the $Ca^{2+}$-free state. The $Ca^{2+}$-induced exposure of the myristoyl group, termed the $Ca^{2+}$-myristoyl switch, enables recoverin to bind to membranes only at high $Ca^{2+}$ levels (*11*, *12*). Our next challenge is to determine the structure of myristoylated recoverin bound to lipid bilayer membranes. It is also of interest to know whether the fatty acyl group is dynamically inserted into the bilayer and determine the precise orientation of the protein relative to the membrane surface.

The atomic resolution structure determination of membrane-bound proteins in general has proven very difficult because membrane proteins are not easily crystallized for X-ray crystallographic analysis. Also, conventional NMR methods require fast rotational correlation times of proteins in solution. The slow reorientation rates of proteins bound to lipid bilayers result in severe broadening of NMR signals, making it very difficult to study membrane-bound proteins using solution NMR techniques.

Solid-state NMR methods are now being developed that overcome the inherent correlation time problem of membrane protein structure determination. Solid-state NMR spectroscopy of aligned samples requires that the proteins be immobilized on a time scale of $10^{-3}-10^{-5}$ $s^{-1}$ and uniaxially oriented with respect to the direction of the applied magnetic field. The lipid bilayers effectively limit the correlation time of the intercalated membrane proteins, and the alignment is achieved mechanically on glass plates with the radio frequency coil wrapped around a stack of plates (*13*, *14*). These samples can be used to measure the orientation-dependent frequencies in NMR spectra that report on the three-dimensional positioning of the peptide planes relative to a molecular frame. The three-dimensional structure can be determined when a sufficient set of spin interactions is collected from the protein in the bilayer environment (*15*, *16*). Solid-state NMR methods have been used to solve the structures of the M2 delta transmembrane fragment of the acetylcholine receptor (*17*), gramicidin A (*18*), transmembrane domain 6 of the α-factor receptor protein (*19*), the transmembrane domain of the M2 protein from influenza A (*20*), and the membrane-bound form of the fd virus coat protein (*21*).

The structure, topology, and dynamics of myristoylated recoverin bound to lipid bilayers were determined by our analysis of solid-state NMR data. The orientation of myristoylated recoverin bound to bilayer membranes was determined by calculating the orientation-dependent solid-state NMR data on the basis of the known structure of $Ca^{2+}$-bound myristoylated recoverin in solution (*10*) and fitting the simulated and experimental spectra. The dynamics of membrane anchoring by the myristoyl chain were inferred from measurements of the $^2H$ NMR order parameters of the deuterated fatty acyl group. These results demonstrate the feasibility of using solid-state NMR to determine the structure and dynamics of a relatively large signaling protein associated with lipid bilayers.

## EXPERIMENTAL PROCEDURES

*Sample Preparation.* All samples were prepared using recombinant myristoylated recoverin produced by coexpressing recoverin and *N*-myristoyl-CoA transferase in *Escherichia coli* (*11*, *22*). Recombinant myristoylated recoverin was expressed and purified as described previously (*11*, *23*). Samples of myristoylated recoverin were uniformly labeled with $^{15}N$ and selectively $^{15}N$-labeled with either [$^{15}N$]leucine or [$^{15}N$]tryptophan as described previously (*24*). A deuterated myristoylated recoverin sample was prepared by growing cells in M9 minimal media supplemented with myristic acid-$d_{28}$ (*24*). Selective [$^{15}N$]leucine and [$^{15}N$]tryptophan labeling was quantified using the solution NMR $^1H-^{15}N$ heteronuclear single-quantum correlation (HSQC)[1] spectra of myristoylated recoverin. The solution NMR assignments (*23*) were used to ascertain the incorporation of the $^{15}N$ labels into the protein and to verify that minimal scrambling of these labels occurred.

Aligned bilayer samples were prepared using 2 mg of the purified protein in a 0.2 mL solution of 10 mM dithiothreitol (DTT), 10 mM $CaCl_2$, and 10 mM HEPES at pH 7.0. The protein solution was added to 35 mg of unilamellar vesicles prepared by tip sonicating a mixture of 80:20 1,2-dioleoyl-*sn*-glycerophosphatidylcholine (DOPC): 1,2-dioleoyl-*sn*-glycerophosphatidylglycerol (DOPG) in 2 mL of water. The final mixture was 79.9:19.9:0.1 mol % DOPC:DOPG:recoverin. The mixture was fast frozen and thawed through five cycles to incorporate the protein into the vesicles. The solution was then dropped onto 20 11 × 11 mm thin glass plates (Marienfeld Inc.) (etched with 50% HF in ethanol) with ~125 μL on each plate. The aqueous solvent was evaporated at 45 °C; then the plates were stacked and hydrated overnight in a closed flask at 94% relative humidity using saturated ammonium phosphate at 45 °C. This temperature exceeds the phase transition temperature of the lipid mixture. The stacked plates were then sealed in parafilm and polyethylene plastic bags for the NMR measurements in a flat coil double-resonance NMR probe.

*Solid-State NMR Spectroscopy.* The solid-state NMR method for structure determination requires that the protein be immobilized and aligned parallel to the direction of the magnetic field. Solid-state $^{31}P$ NMR spectra confirmed the orientation of the phosphate group of the DOPC/DOPG lipid bilayers. $^2H$ NMR spectra of $d_{28}$ myristoylated recoverin

[1] Abbreviations: HSQC, heteronuclear single-quantum coherence; PISEMA, polarization inversion with spin exchange at the magic angle; DOPC, 1,2-dioleoyl-*sn*-glycerophosphatidylcholine; DOPG, 1,2-dioleoyl-*sn*-glycerophosphatidylglycerol; DMPC, dimyristoylphosphatidylcholine; DTT, dithiothreitol; HEPES, *N*-(2-hydroxyethyl)piperazine-*N*′-2-ethanesulfonic acid.

confirm the orientation and report on the dynamics of the myristoyl group within the oriented bilayer. Solid-state $^{15}N$ NMR spectra report on the orientation of the protein backbone in the lipid bilayer.

The solid-state NMR experiments were performed on a home-built NMR spectrometer with a 700/62 Magnex magnet (Magnex Scientific Ltd., Oxfordshire, U.K.). The double-resonance $^{1}H$ and $^{15}N$ probe had coil dimensions of $11 \times 11 \times 3$ mm; a separate probe double tuned for $^{1}H$ and $^{31}P$ was used for the $^{31}P$ NMR measurements (*14*). A flat coil single-tuned probe was used for the $^{2}H$ NMR experiments. One-dimensional $^{31}P$ NMR spectra were recorded using a single pulse experiment with $^{1}H$ decoupling during acquisition. The $^{31}P$ chemical shift frequencies were measured relative to external 85% phosphoric acid at 0 ppm. One-dimensional $^{15}N$ NMR spectra were recorded using the mismatch optimized (CPMOIST) cross-polarization technique (*25*, *26*), with a 52 kHz cross-polarization field strength and 62.5 kHz $^{1}H$ decoupling field strength during the 5 ms acquisition time. A total of 1000 transients for uniformly $^{15}N$-labeled recoverin and 10000 transients for selectively labeled [$^{15}N$]leucine- or [$^{15}N$]tryptophan-labeled recoverin were signal averaged. A recycle time of 7 s was used to prevent radio frequency heating of the hydrated samples. The temperature was controlled at 5 °C. The $^{15}N$ chemical shift frequencies were measured relative to external ammonium at 0 ppm. A quadrupole echo sequence (*27*) was used to acquire the $^{2}H$ NMR spectra at 5 °C. The echo time was set to 45 $\mu$s using a 90 kHz field strength for the irradiation pulses. A recycle time of 0.2 s was used for the signal averaging of 500000 transients.

The two-dimensional PISEMA spectra (*28*) were obtained using similar field strengths and signal averaging conditions as in the one-dimensional experiments. The frequency-switched Lee−Goldberg condition was set up with a 34.5 kHz frequency jump to effect the $^{1}H$ spin lock at the magic angle. The $^{1}H-^{15}N$ dipolar frequency was allowed to evolve for 64 $t_1$ increments for a total evolution in the dipolar dimension of 2.5 ms. The two-dimensional data set was processed using Felix97 (Accelrys, San Diego, CA). The data were zero filled twice in both the $t_2$ dimension and the $t_1$ dimension yielding a $512 \times 512$ real matrix. The apodization in $t_2$ was a 400 Hz exponential multiplication; a sine bell was applied in $t_1$.

*Calculation of PISEMA Spectra.* The spectroscopic method for protein structure determination relies on the measurement of several orientation-dependent frequencies from peptide backbone sites. These include the $^{15}N$ chemical shift and the $^{1}H-^{15}N$ dipolar interactions. The two-dimensional PISEMA experiment (*28*) correlates the $^{15}N$ chemical shift frequency with the $^{1}H-^{15}N$ dipolar frequency, and each correlation peak in the PISEMA spectrum therefore represents a unique orientation of an individual backbone amide site. The orientation of the peptide plane relative to the magnetic field can then be calculated from the $^{15}N$ chemical shift and $^{1}H-^{15}N$ dipolar frequencies (see Figure 1 and eqs 1 and 2 below). Hence, the observed PISEMA spectrum can be calculated from the orientations of each of the 189 peptide planes in the molecule or any subset of those peptide planes at any given orientation of the molecule. The agreement between the experimental and simulated PISEMA spectra forms the basis for the determination of the molecular orientation relative to the surface of the lipid bilayer (*29*).

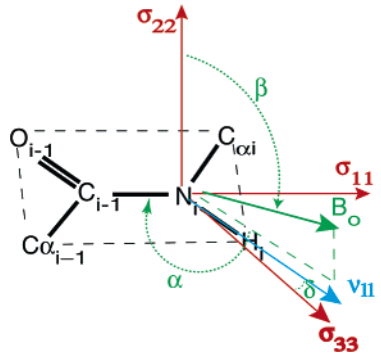


FIGURE 1: Representation of the angles relating the $^{15}N$ CSA principal axis system to the laboratory axis frame for a peptide bond, the $^{15}N$ CSA principal axis system ($\sigma_{11}$, $\sigma_{22}$, $\sigma_{33}$) relative to the molecular frame, and the $^{1}H-^{15}N$ dipolar principal axis system ($\nu_{||}$) relative to the molecular frame.

The nuclear spin interactions are anisotropic and are described by second rank tensors. Principal elements defining the second rank tensor of the chemical shift anisotropy (CSA) are measured as the discontinuities in the powder pattern line shape of the NMR spectrum of an unoriented sample. The relation of this second rank tensor to the molecular frame (the orientation of the peptide plane) is described by a set of Euler angles relating the two axis systems. The orientation of the $^{15}N$ amide chemical shift tensor in the molecular frame has been determined from model peptides and verified in protein studies (*30*). The $^{15}N$ chemical shift frequency is evaluated according to the equation:

$$\sigma_{obs} = \sigma_{11} \sin^2(\alpha - \delta) \sin^2\beta + \sigma_{22} \cos^2\beta + \sigma_{33} \cos^2(\alpha - \delta) \sin^2\beta \quad (1)$$

where $\sigma_{11}$, $\sigma_{22}$, and $\sigma_{33}$ are the principal elements of the CSA tensor, $\alpha$ and $\beta$ are the Euler angles relating the orientation of the peptide plane to the laboratory frame, and $\delta$ is the angle between the HN bond and the $\sigma_{33}$ axis in the peptide plane. The $^{1}H-^{15}N$ dipolar interaction is described by a second rank tensor with one of the elements of the principal axis system lying along the bond vector connecting the two nuclei. The dipolar interaction results in a doublet, with maximal splitting when the bond vector is aligned parallel to the applied field and half-maximal splitting when the bond vector is aligned perpendicular to the applied field. The evaluation of the orientational parameter from the dipolar splitting is given by

$$\Delta\nu_D = \nu_{||}(3 \sin^2\beta \cos^2\alpha - 1) \quad (2)$$

where $\nu_{||} = \mu_0 h \gamma_I \gamma_S / 8\pi^3 r^3$; $\mu_0$ is the vacuum permeability, $h$ is Planck's constant, and $\gamma_I$ and $\gamma_S$ are the gyromagnetic ratios of the $^{1}H$ and $^{15}N$ nuclei, respectively. This is shown in Figure 1.

The calculation of the two-dimensional PISEMA spectra was performed using the previously determined structure of myristoylated recoverin in the presence of $Ca^{2+}$ (*10*). The program SIMSPEC was used to find the best fit of the experimental PISEMA data to the set of $^{15}N$ chemical shifts and $^{1}H-^{15}N$ dipolar couplings calculated from this structure. The orientations are taken relative to the *Z* axis, arbitrarily

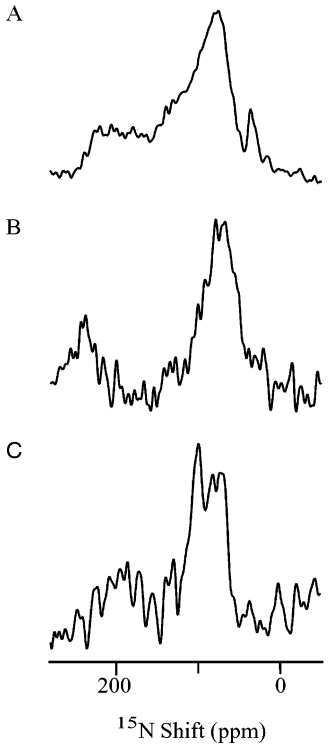


FIGURE 2: One-dimensional solid-state $^{15}$N NMR spectra of myristoylated recoverin associated with membrane bilayers. (A) Uniformly $^{15}$N-labeled myristoylated recoverin aligned in DOPC−DOPG bilayers. (B) Selective [$^{15}$N]leucine-labeled myristoylated recoverin in aligned DOPC−DOPG bilayers. (C) Selective [$^{15}$N]tryptophan-labeled myristoylated recoverin in aligned DOPC−DOPG bilayers.

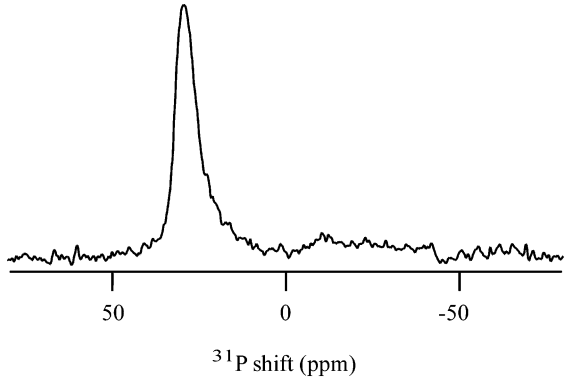


FIGURE 3: One-dimensional $^{31}$P NMR spectrum of the selective [$^{15}$N]Trp-labeled myristoylated recoverin in aligned POPC−POPG bilayers.

chosen as the magnetic field direction in the coordinate file. The set of angles $\alpha$ and $\beta$ are evaluated from the three-dimensional coordinates of the model, and the $^{15}$N CSA and $^{1}$H−$^{15}$N dipolar frequencies are calculated from these angles for each peptide backbone site. The calculated set results in the correlation frequencies of the PISEMA experiment. Importantly, this set can be simulated for all of the peptide planes in the protein or for any subset of residues. A grid search is performed over all possible orientations of the protein relative to the magnetic field, enabling the agreement between the simulated chemical shift and dipolar coupling frequencies and the set of experimentally measured values to be assessed for each orientation. The chemical shifts and dipolar couplings were weighted equally. For each experimental resonance, due to the lack of residue-specific assignment, the closest calculated point is chosen as the corresponding point in order to calculate the fit score. This process was continued through all possible tilt and rotation angles in increments of 1°. Calculated PISEMA spectra were then evaluated for their similarity to the experimental PISEMA spectrum. Visualization of the protein structure relative to the magnetic field was displayed using InsightII (Accelrys, San Diego, CA).

## RESULTS

One-dimensional $^{15}$N NMR spectra of myristoylated recoverin bound to DOPC−DOPG lipid bilayers are shown in Figure 2. The spectrum of uniformly $^{15}$N myristoylated labeled recoverin (Figure 2A) results from many overlapping single-line resonances with chemical shift frequencies that span the full breadth of a powder pattern, as expected for a large protein with a reasonable distribution of secondary structural elements. However, the powder pattern line shape itself is not represented because the distribution of orientations is not completely random. Thus, the one-dimensional spectrum by itself provides evidence that the protein is bound to the aligned lipid bilayers with a well-defined orientation. The spectrum of myristoylated recoverin selectively labeled with [$^{15}$N]leucine (Figure 2B) has resonances from the 16 leucine residues only. The majority of these resonances are near the $\sigma_{11}$ and $\sigma_{22}$ discontinuities of the powder pattern, indicating that most of the leucine residues have amide N−H bonds oriented approximately perpendicular to the applied field and the bilayer normal. There are also a few leucine residues with resonances near the $\sigma_{33}$ discontinuity, associated with N−H amide bond vectors approximately parallel to the bilayer normal. The NMR spectrum of the selectively [$^{15}$N]tryptophan-labeled myristoylated recoverin (Figure 2C) indicates the amide N−H bonds of the three Trp residues (W31, W104, and W156) are near the $\sigma_{11}$, $\sigma_{22}$ discontinuties of the powder pattern. The one-dimensional $^{15}$N NMR spectra serve as coarse indicators of the orientations of the labeled sites. Two-dimensional NMR spectra are necessary to resolve resonances and to enable quantification of the protein structure and orientation.

The alignment of the protein-containing lipid bilayers on glass plates is confirmed by the $^{31}$P NMR spectrum shown in Figure 3. The observed $^{31}$P resonance frequency corresponds to the parallel component of the motionally averaged axially symmetric chemical shift tensor of a phosphate group rotating about its O−P−O axis (*31*).

The properties of the myristoyl group were characterized by $^{2}$H NMR spectra of $d_{28}$ myristoylated recoverin bound to aligned DOPC−DOPG bilayers. It was first necessary to investigate the behavior of a $^{2}$H-labeled phospholipid (DMPC), representative of a myristoyl chain buried inside the bilayer. The spectra in Figure 4 show the full spectral width sampled by the $^{2}$H quadrupole interaction from the methylene and terminal methyl groups of a hydrated fully deuterated DMPC incorporated into a lipid bilayer. The spectrum in Figure 4A of unoriented hydrated DMPC-$d_{56}$:DOPC:DOPG lipids in a ratio of 10:72:18 shows a superposition of the doublets for the $^{2}$H quadrupole splitting from each of the motionally averaged methylene and terminal methyl sites (*32*). The edges

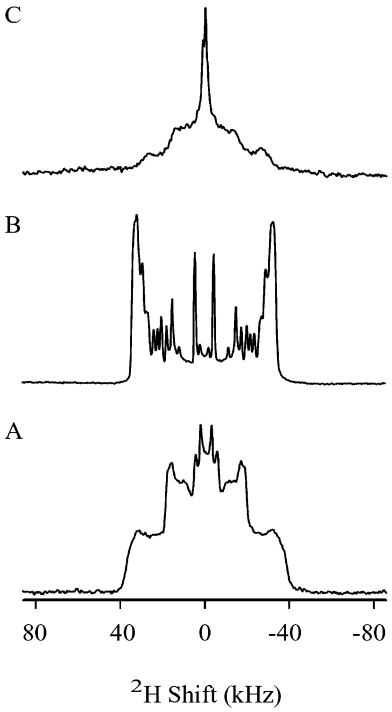


FIGURE 4: One-dimensional $^2$H NMR spectra. (A) DMPC-$d_{56}$ in unoriented DOPC−DOPG bilayers at 5 °C. (B) DMPC-$d_{56}$ in aligned DOPC−DOPG bilayers at 5 °C. (C) $d_{28}$ myristoylated recoverin in aligned DOPC−DOPG bilayers at 5 °C.

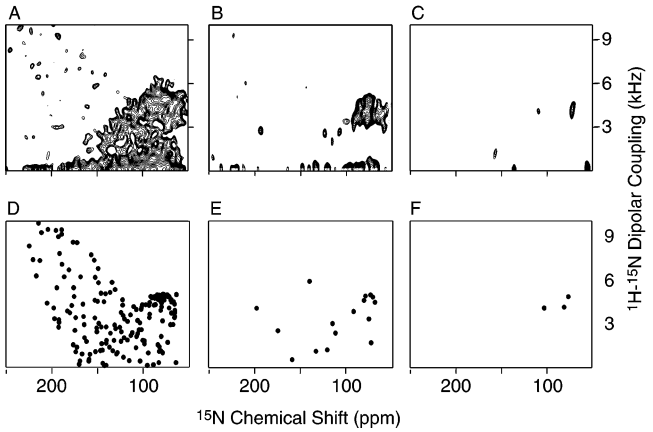


FIGURE 5: Two-dimensional aligned $^{15}$N chemical shift/$^1$H−$^{15}$N dipolar PISEMA spectra of myristoylated recoverin oriented in POPC−POPG bilayers. (A) Uniformly $^{15}$N-labeled myristoylated recoverin. (B) [$^{15}$N]Leucine-labeled myristoylated recoverin. (C) [$^{15}$N]Tryptophan-labeled myristoylated recoverin. In all of the spectra, the zero frequency distortion along the bottom of the PISEMA spectra is not included in the fitting. The four weak peaks in the upper left quadrant of the [$^{15}$N]Leu spectrum and the weak peak in the bottom left of the [$^{15}$N]Trp were not included on the basis of the one-dimensional $^{15}$N spectra. (D) Calculated PISEMA spectrum showing all resonances with the PDB coordinate file rotated 247° about the *X* axis and then tilted 62° about the *Y* axis. (E) Calculated PISEMA spectrum showing only resonances from leucine residues. (F) Calculated PISEMA spectrum showing only resonances from tryptophan residues.

of the spectrum are at ±32.3 kHz, which corresponds to an order parameter *S* of 0.39 for the least motionally averaged sites, presumably the methylene group at position C2 along the chain. The order parameters decrease as the chain position increases to the most motionally averaged site at the terminal methyl group. This site contributes the narrowest component with an outer splitting of 4.89 kHz, corresponding to an order parameter of 0.06. The spectrum for the same lipid composition aligned on glass plates exhibits resolved individual frequencies for the various splittings (Figure 4B). The outer discontinuity of the doublet corresponds to the lipid chain aligned along the bilayer normal (*33*). The quadrupole splittings can be measured uniquely for 12 of the 14 methylene groups of the myristoyl chain. The spectrum of $d_{28}$ myristoylated recoverin associated with aligned DOPC−DOPG bilayers (Figure 4C) reveals that the myristoyl group has a decreased overall order parameter relative to the DMPC in DOPC−DOPG bilayers alone. For example, the order parameter of the outer edge is observed to be $S = 0.33$, which corresponds to an approximately 15% increase in mobility of the myristoyl group attached to the recoverin compared to that attached to a phosphatidylcholine headgroup. Therefore, the myristoyl group of recoverin does not appear to be completely aligned in the bilayer and appears to be more motionally averaged than the equivalent chain positions in the DMPC in bilayers.

Two-dimensional PISEMA spectra of $^{15}$N-labeled samples of myristoylated recoverin associated with aligned lipid bilayers are shown in Figure 5. These spectra are substantially different than a powder pattern. There is increased intensity along the $\sigma_{11}$, $\sigma_{22}$ edge of the spectrum for the uniformly $^{15}$N-labeled recoverin (Figure 5A). The resonances in this spectrum are overlapped, making it difficult to analyze. However, the spectra of samples containing selective labeling of [$^{15}$N]leucine (Figure 5B) and [$^{15}$N]tryptophan (Figure 5C) are more tractable and enable orientations of the 16 leucine and 3 tryptophan residues to be analyzed. In particular, the spectrum of the [$^{15}$N]Trp-labeled recoverin has three resonances that represent the amide backbone sites of the 3 Trp residues. Individual resonances can be recognized for many of the leucine residues. These two data sets were used as the basis for the fit of the orientation of the protein structure. Because the residue-specific assignments of these spectra are not determined experimentally, the closest calculated peak is assigned as the corresponding residue. Regardless, enforcing the quantitative agreement between the experimental and calculated spectra severely limits the range of possible orientations for the proteins.

The fitting of the solid-state NMR data to simulated spectra derived from the previously determined solution NMR structure of myristoylated recoverin was carried out using the program SIMSPEC. The input consisted of the PDB coordinates of $Ca^{2+}$-bound myristoylated recoverin; the PDB file used in our analysis was structure number 3 from 1JSA.PDB (*10*). The initial orientation of the protein structure used in the calculation was arbitrarily taken as the orientation of the PDB file. The structure was systematically rotated about the laboratory *X* and *Y* axes in 1° increments, sampling all possible orientations of the protein to determine the one with the best fit to the observed PISEMA data. Since the axis of alignment of the bilayers is about the laboratory *Z* axis (for our purposes parallel to $B_o$), the result is invariant for rotations about *Z*. The calculated PISEMA spectra for the selectively [$^{15}$N]Leu-labeled myristoylated recoverin and the selectively [$^{15}$N]Trp-labeled myristoylated recoverin were used together to evaluate which orientation results in the best fit to the experimental PISEMA spectrum. Independent results of the orientation derived from the two selectively

Table 1: Calculated and Experimental Resonance Parameters of [$^{15}$N]Leu and [$^{15}$N]Trp Recoverin[a]

| calculated | | observed | |
|---|---|---|---|
| $^{15}$N shift (ppm) | dipolar coupling (kHz) | $^{15}$N shift (ppm) | dipolar coupling (kHz) |
| | | [$^{15}$N]Leu | |
| 198 | 4.10 | 193.93 | 3.35 |
| 175 | 2.54 | | |
| 159 | 0.57 | | |
| 141 | 5.93 | 141.23 | 5.71 |
| 133 | 1.20 | | |
| 121 | 2.36 | 123.70 | 3.10 |
| 115 | 3.03 | 115.56 | 2.49 |
| 112 | 2.36 | 107.49 | 3.21 |
| 92 | 3.86 | 99.23 | 4.09 |
| 82 | 4.57 | 90.56 | 4.21 |
| 80 | 4.93 | 78.19 | 5.51 |
| 76 | 3.34 | 76.24 | 4.87 |
| 75 | 5.01 | 68.27 | 5.53 |
| 74 | 1.74 | | |
| 72 | 4.86 | 66.63 | 4.57 |
| 69 | 4.50 | 65.63 | 4.44 |
| | | [$^{15}$N]Trp | |
| 103 | 4.05 | 108.67 | 3.98 |
| 80 | 4.06 | 72.93 | 4.11 |
| 76 | 4.81 | 72.93 | 4.11 |

[a] Observed $^{15}$N shifts and dipolar couplings for [$^{15}$N]Leu (Figure 5B) and [$^{15}$N]Trp (Figure 5C) and the corresponding calculated values from Figure 5E,F.

labeled samples were then compared to verify that the orientation is consistent with both data sets. The orientation that provides the best fit to both the $^{1}$[$^{15}$N]Trp (Figure 5B) and [$^{15}$N]Leu (Figure 5C) spectra was derived using the linear distances scoring algorithm of SIMSPEC. The best fit corresponds to the PDB structure file (1JSA.PDB) rotated 247° about the *X* axis and then tilted 62° about the *Y* axis (Figure 5D,E and Table 1).

Calculated PISEMA spectra for three different orientations of myristoylated recoverin are shown in Figure 6. The calculated spectra vary significantly as a function of the orientation of the protein. The calculated PISEMA spectra in Figure 6A−C correspond to the orientation that optimally fits the spectrum of the Trp selective label alone (Figure 5B). The calculated spectra in Figure 6D−F correspond to the orientation that best fits the spectrum of the Leu selective label alone (Figure 5C). The calculated spectra in Figure 6G−I correspond to an arbitrary orientation that has no correspondence with the experimental data. Hence, the calculated spectra in Figure 6 illustrate that small differences in the orientation of the bound protein result in relatively large spectral changes.

The final convergent orientation and structure of myristoylated recoverin bound to the oriented phospholipid bilayer is illustrated in Figure 7. The long molecular axis of recoverin is oriented ~45° with respect to the membrane normal. The N-terminus of the protein points toward the membrane surface with the myristoyl group positioned deeply inside the lipid bilayer. In addition, the amino-terminal helix (shown in pink in Figure 7, residues L9−L17) lies flat along the membrane surface and appears to make very intimate contact with membrane headgroups. The $Ca^{2+}$ ion bound to the second EF-hand of recoverin is spatially close to the membrane surface and may interact electrostatically with the negatively charged headgroups.

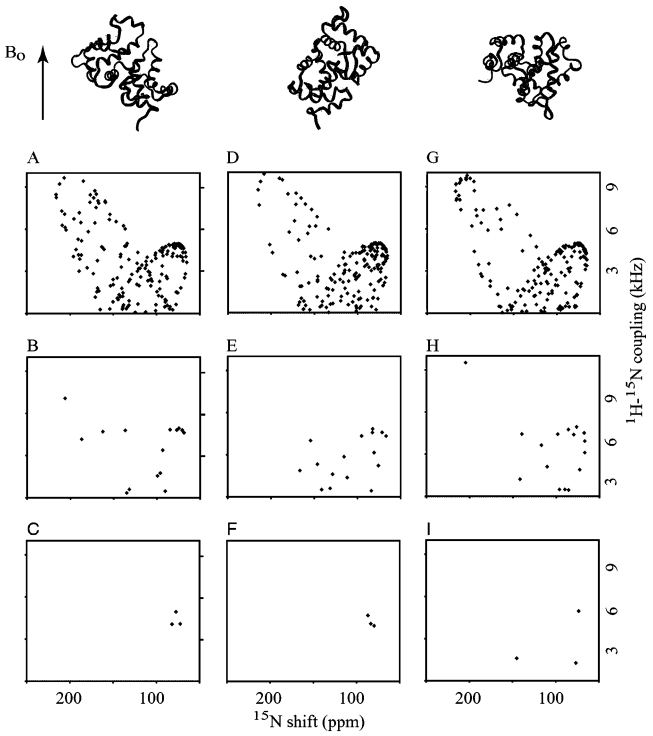


FIGURE 6: Calculated PISEMA spectra of myristoylated recoverin at various alignments relative to the magnetic field. The calculated spectra for all residues (top), leucine (middle), and tryptophan (bottom) are shown for three different orientations: the best Trp fit is for a rotation of 138° and a tilt of 133° (A−C); the best Leu fit is for a rotation of 136° and a tilt of 92° (D−F); an arbitrary orientation with no correspondence to the data with a rotation of 45° and a tilt of 45° (G−I). The top panel indicates the orientation of the structure relative to the bilayer normal.

## DISCUSSION

Myristoylated recoverin binds to bilayer membranes with a single fixed orientation that retains the three-dimensional fold of the protein in solution. Surprisingly, the protein is oriented such that relatively few residues of the protein make very close contact with the membrane surface. The basic residues (K5, K11, K37, R43, and K84) in the amino-terminal domain are solvent exposed and form positively charged sites that make relatively close contact (<6 Å) with the negatively charged phospholipid headgroups at the membrane surface (Figures 7 and 8). This electrostatic interaction may contribute somewhat to the overall energetics of membrane binding and complement the hydrophobic anchoring of the myristoyl group, similar to that seen for other myristoyl switch proteins such as Src and the MARCKS protein (*34*, *35*). Basic residues in the C-terminal tail of recoverin (eight positively charged side chains in the last 23 residues) do not make contact with the membrane surface, in contrast to suggestions from an earlier report that these residues might be important for the binding of recoverin to membranes (*36*). The N-terminal myristoyl group, as expected, appears to be inserted directly inside the hydrophobic region of the lipid bilayer (Figures 7 and 8). However, our $^{2}$H NMR order parameter analysis suggests that the myristoyl group may not be completely aligned along with fatty acyl groups in the bilayer and may be somewhat disordered. Consistent with this interpretation, retinal rod outer segment disk membranes contain an abundance of polyunsaturated

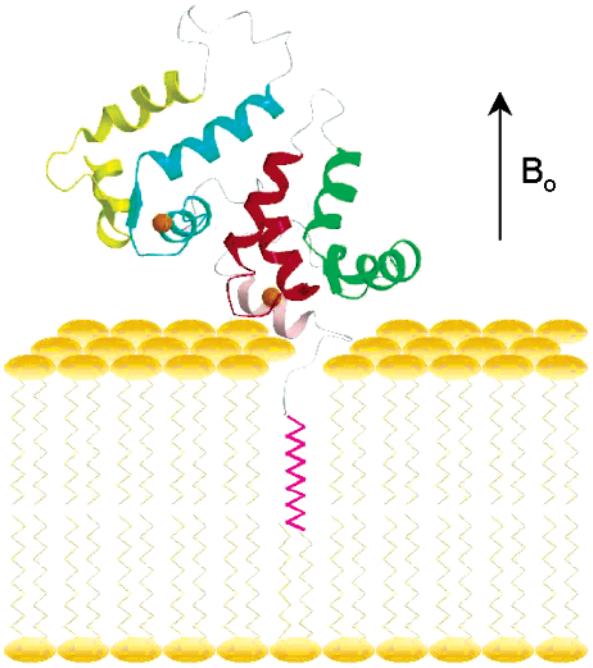


FIGURE 7: Ribbon representation of the main chain structure of $Ca^{2+}$-bound myristoylated recoverin situated in the lipid bilayer according to the solid-state NMR results (PDB structure file rotated to $X = 247°$ and $Y = 62°$). The four EF-hand motifs are highlighted in green (EF-1), red (EF-2), cyan (EF-3), and yellow (EF-4), bound $Ca^{2+}$ ions are in orange, N-terminal helix is in pink, and the N-terminal myristoyl group (magenta) is modeled schematically inside the bilayer.

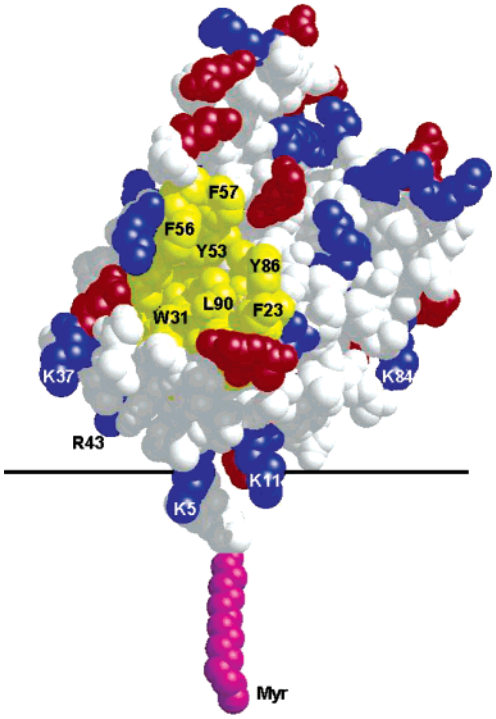


FIGURE 8: Space-filling representation of myristoylated recoverin bound schematically to a membrane with the orientation determined from the solid-state NMR results (same view as in Figure 7 except rotated ~180° about the bilayer normal). The N-terminal myristoyl group (magenta) is modeled inside the membrane. Solvent-exposed hydrophobic side chains are in yellow, and charged side chains are highlighted in red and blue.

fatty acids (e.g., C22:6), suggesting that the native disk membranes are quite fluid and disordered (*37*, *38*).

The structure of membrane-bound recoverin reveals a solvent-exposed hydrophobic crevice that may serve as a potential binding site for the target protein, rhodopsin kinase (Figure 8). In particular, the exposed crevice is lined by many aromatic residues (F23, W31, F35, F49, Y53, F56, F57, Y86, and L90) that are highly conserved in all homologues of recoverin (*39*, *40*). Interestingly, many of these exposed aromatic groups make intimate contacts with the sequestered myristoyl group in the structure of the $Ca^{2+}$-free protein (*9*, *10*, *41*). The $Ca^{2+}$-induced extrusion of the myristoyl group causes these hydrophobic residues to become solvent exposed in the $Ca^{2+}$-bound protein, making them available to interact with the target, rhodopsin kinase. In addition, an outer ring of charged residues surrounds the hydrophobic crevice. Perhaps these nonconserved charged residues might play a role in target specificity. The hydrophobic and charged residues highlighted in Figure 8 have been shown previously to affect target binding as demonstrated by site-directed mutagenesis analysis (*42*, *43*).

The $^{15}N$ chemical shifts and $^{1}H-^{15}N$ dipolar coupling frequencies observed in solid-state NMR spectra of aligned samples provide sufficient information to calculate the orientation of proteins bound to membranes. In our study of recoverin, the assignments of the experimental solid-state spin interaction frequencies for all residues of recoverin are consistent with those assignments predicted from the known structure in solution. Therefore, a strong correlation exists between the experimental PISEMA data set and the calculated best-fit spectrum. The fit of the back-calculated solid-state NMR PISEMA spectrum to the solution NMR structure suggests that the overall structure of recoverin bound to oriented bilayer membranes is very similar to that of recoverin in solution (*10*). Hence, membrane binding by recoverin is achieved by insertion of the myristoyl group inside the bilayer, with apparently little rearrangement of protein structure.

In summary, we have demonstrated that myristoylated recoverin can be mechanically oriented in bilayers on glass plates with the myristoyl chain anchoring the protein in the lipid bilayer. The dynamics of the myristoylated chain indicate a moderate decrease in the order parameter relative to the phospholipids in the surrounding bilayer, suggesting a highly fluid chain behavior. The myristoyl chain does not show the same degree of alignment as the surrounding bilayer, suggesting a local disruption of the bilayer to accommodate the protein insertion. The protein, however, demonstrates a highly aligned conformation relative to the bilayer as evidenced by the one to one correlation of amide backbone sites in the oriented PISEMA spectra.

## REFERENCES

1. Wilcox, C., Hu, J. S., and Olson, E. N. (1987) *Science 238*, 1275−1278.
2. Gordon, J. I., Duronio, R. J., Rudnick, D. A., Adams, S. P., and Gokel, G. W. (1991) *J. Biol. Chem. 266*, 8647−8650.
3. Kamps, M. P., Buss, J. E., and Sefton, B. M. (1985) *Proc. Natl. Acad. Sci. U.S.A. 82*, 4625−4628.
4. Dizhoor, A. M., Ray, S., Kumar, S., Niemi, G., Spencer, M., Rrolley, D., Walsh, K. A., Philipov, P. P., Hurley, J. B., and Stryer, L. (1991) *Science 251*, 915−918.
5. Polans, A., Baehr, W., and Palczewski, K. (1996) *Trends Neurosci. 19*, 547−554.

6. Palczewski, K., Polans, A. S., Baehr, W., and Ames, J. B. (2000) *BioEssays 22*, 337−350.
7. Erickson, M. A., Lagnado, L., Zozulya, S., Neubert, T. A., Stryer, L., and Baylor, D. A. (1998) *Proc. Natl. Acad. Sci. U.S.A. 95*, 6474−6479.
8. Kawamura, S. (1993) *Nature 362*, 855−857.
9. Tanaka, T., Ames, J. B., Harvey, T. S., Stryer, L., and Ikura, M. (1995) *Nature 376*, 444−447.
10. Ames, J. B., Ishima, R., Tanaka, T., Gordon, J. I., Stryer, L., and Ikura, M. (1997) *Nature 389*, 198−202.
11. Zozulya, S., and Stryer, L. (1992) *Proc. Natl. Acad. Sci. U.S.A. 89*, 11569−11573.
12. Dizhoor, A. M., Chen, C. K., Olshevskaya, E., Sinelnikova, V. V., Phillipov, P., and Hurley, J. B. (1993) *Science 259*, 829−832.
13. Teng, Q., Nicholson, L. K., and Cross, T. A. (1991) *J. Mol. Biol. 218*, 607.
14. Bechinger, B., and Opella, S. J. (1991) *J. Magn. Reson. 95*, 585−587.
15. Opella, S. J., Stewart, P. L., and Valentine, K. V. (1987) *Q. Rev. Biophys. 19*, 7−49.
16. Cross, T. A., and Opella, T. A. (1994) *Curr. Opin. Struct. Biol. 4*, 574−581.
17. Opella, S. J., Gesell, J., Valente, A. P., Marassi, F. M., Pblatt-Montal, M., Sun, W., Ferrer-Montiel, A., and Montal, M. (1997) *Chemtracts: Biochem. Mol. Biol. 10*, 153−174.
18. Ketchem, R., Hu, W., and Cross, T. A. (1993) *Science 261*, 1457−1460.
19. Valentine, K. G., Liu, S. F., Marassi, F. M., Veglia, G., Opella, S. J., Ding, F. X., Wang, S. H., Arshava, B., Becker, J. M., and Naider, F. (2001) *Biopolymers 59*, 243−256.
20. Wang, J., Kim, S., Kovacs, F., and Cross, T. A. (2001) *Protein Sci. 10*, 2241−2250.
21. Marassi, F. M., and Opella, S. J. (2003) *Protein Sci. 12*, 403−411.
22. Ray, S., Zozulya, S., Niemi, G. A., Flaherty, K. M., Brolley, D., Dizhoor, A. M., McKay, D. B., Hurley, J., and Stryer, L. (1992) *Proc. Natl. Acad. Sci. U.S.A. 89*, 5705−5709.
23. Ames, J. B., Tanaka, T., Stryer, L., and Ikura, M. (1994) *Biochemistry 33*, 10743−10753.
24. Tanaka, T., Ames, J. B., Kainosho, M., Stryer, L., and Ikura, M. (1998) *J. Biomol. NMR 11*, 135−152.
25. Levitt, M. H., Suter, D., and Ernst, R. R. (1986) *J. Chem. Phys. 84*, 4243−4255.
26. Pines, A., Gibby, M. G., and Waugh, J. S. (1973) *J. Chem. Phys. 59*, 569−590.
27. Davis, J. H., Jeffrey, K. R., Bloom, M., Valie, M. I., and Higgs, T. P. (1976) *Chem. Phys. Lett. 42*, 390−394.
28. Wu, C. H., Ramamoorthy, A., and Opella, S. J. (1994) *J. Magn. Reson. 109*, 270−272.
29. Mesleh, M. F., Valentine, K. G., Opella, S. J., Louis, J. M., and Gronenborn, A. M. (2003) *J. Biomol. NMR 25*, 55−61.
30. Wu, C. H., Ramamoorthy, A., Gierasch, L. M., and Opella, S. J. (1995) *J. Am. Chem. Soc. 117*, 6148−6149.
31. Herzfeld, J., Griffin, R. G., and Haberkorn, R. A. (1978) *Biochemistry 17*, 2711−2718.
32. Davis, J. H. (1981) *Biochim. Biophys. Acta 737*, 117−171.
33. Prosser, R. S., Hwang, J. S., and Vold, R. R. (1998) *Biophys. J. 75*, 2405−2418.
34. McLaughlin, S., and Aderem, A. (1995) *Trends Biochem. Sci. 20*, 272−276.
35. Sigal, C. T., Zhou, W., Buser, C. A., McLauglin, S., and Resh, M. D. (1994) *Proc. Natl., Acad. Sci. U.S.A. 91*, 12253−12257.
36. Matsuda, S., Hisatomi, O., and Tokunaga, F. (1999) *Biochemistry 38*, 1310−1315.
37. Johnson, R. S., Ohguro, H., Palczewski, K., Hurley, J. B., Walsh, K. A., and Neubert, T. A. (1994) *J. Biol. Chem. 269*, 21067−21071.
38. Uauy, R., Hoffman, D. R., Peirano, P., Birch, D. G., and Birch, E. E. (2001) *Lipids 36*, 885−895.
39. Ames, J. B., Tanaka, T., Stryer, L., and Ikura, M. (1996) *Curr. Opin. Struct. Biol. 6*, 432−438.
40. Burgoyne, R. D., and Weiss, J. L. (2001) *Biochem. J. 353*, 1−12.
41. Ames, J. B., Hamasaki, N., and Molchanova, T. (2002) *Biochemistry 41*, 5776−5787.
42. Tachibanaki, S., Nanda, K., Sasaki, K., Ozaki, K., and Kawamura, S. (2000) *J. Biol. Chem. 275*, 3313−3319.
43. Olshevskaya, E. V., Boikov, S., Ermilov, A., Krylov, D., Hurley, J. B., and Dizhoor, A. M. (1999) *J. Biol. Chem. 274*, 10823−10832.

BI0206816